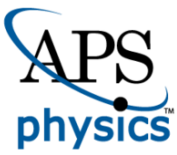

This is the accepted manuscript made available via CHORUS. The article has been published as:

Using Λ_{b}→Λμ^{+}μ^{-} data within a Bayesian analysis of |ΔB|=|ΔS|=1 decays

Stefan Meinel and Danny van Dyk

Phys. Rev. D **94**, 013007 — Published 13 July 2016

DOI: 10.1103/PhysRevD.94.013007

Using $\Lambda_b \to \Lambda\mu^+\mu^-$ data within a Bayesian analysis of $|\Delta B| = |\Delta S| = 1$ decays

Stefan Meinel*
Department of Physics, University of Arizona, Tucson, AZ 85721, USA and
RIKEN BNL Research Center, Brookhaven National Laboratory, Upton, NY 11973, USA

Danny van Dyk†
Physik-Institut, Universität Zürich, Winterthurer Strasse 190, 8057 Zürich, Switzerland

We study the impact of including the baryonic decay $\Lambda_b \to \Lambda(\to p\pi^-)\mu^+\mu^-$ in a Bayesian analysis of $|\Delta B| = |\Delta S| = 1$ transitions. We perform fits of the Wilson coefficients $\mathcal{C}_9$, $\mathcal{C}_{9'}$, $\mathcal{C}_{10}$ and $\mathcal{C}_{10'}$, in addition to the relevant nuisance parameters. Our analysis combines data for the differential branching fraction and three angular observables of $\Lambda_b \to \Lambda(\to p\pi^-)\mu^+\mu^-$ with data for the branching ratios of $B_s \to \mu^+\mu^-$ and inclusive $b \to s\ell^+\ell^-$ decays. Newly available precise lattice QCD results for the full set of $\Lambda_b \to \Lambda$ form factors are used to evaluate the observables of the baryonic decay. Our fits prefer shifts to $\mathcal{C}_9$ that are opposite in sign compared to those found in global fits of only mesonic decays, and the posterior odds show no evidence of physics beyond the Standard Model. We investigate a possible hadronic origin of the observed tensions between theory and experiment.

I. INTRODUCTION

The tensions between theory and experiment for P_5' [1, 2], one of the angular observables in the kinematical distribution of the decay $\bar{B} \to \bar{K}^*(\to \bar{K}\pi)\mu^+\mu^-$ [3], have sparked much interest in the determination of the short-distance couplings in flavor-changing neutral currents of the form $b \to s\ell^+\ell^-$. Several competing global analyses have been published [4–14] that use the available data on such rare decays of $\bar{B}$ mesons to various degrees, and most of these analyses find that a negative shift in the Wilson coefficient $\mathcal{C}_9$ improves the agreement with the data. However, it remains unclear whether this effect is caused by physics beyond the Standard Model, or merely by uncontrolled hadronic contributions.

None of the published analyses include the first measurements of angular observables of the baryonic rare decay $\Lambda_b \to \Lambda(\to p\pi^-)\mu^+\mu^-$ [15], which offers complementary constraints compared to the commonly used mesonic channels. A recent lattice QCD calculation of the relevant $\Lambda_b \to \Lambda$ form factors [16] enables us to evaluate the $\Lambda_b \to \Lambda(\to p\pi^-)\mu^+\mu^-$ observables with high precision. The purpose of this work is thus to study the constraining power of the b-baryon decay in a global analysis of $|\Delta B| = |\Delta S| = 1$ decays.

Our article is structured as follows: First, we briefly describe our framework, define our fit models and review the observations that enter our likelihood function in section II. We then present our results for each of the fit models in section III, and further discuss the implications in section IV. Appendix A describes the subleading corrections to the OPE at low hadronic recoil; appendix B gives posterior-predictive distributions for the full set of $\Lambda_b \to \Lambda(\to p\pi^-)\mu^+\mu^-$ angular observables, and appendix C contains additional fit results using only the data for the baryonic decay.

II. FRAMEWORK

We work in the usual effective field theory for flavor-changing neutral $b \to s\{\gamma, \ell^+\ell^-\}$ transitions; see e.g. [17]. Its Hamiltonian reads

$$\begin{aligned}\mathcal{H}_{\text{eff}} = &-\frac{4\,G_F}{\sqrt{2}} V_{tb}V_{ts}^* \frac{\alpha_e}{4\pi} \sum_i \mathcal{C}_i(\mu)\mathcal{O}_i \\ &+ \mathcal{O}\left(V_{ub}V_{us}^*\right) + \text{h.c.}\,,\end{aligned} \tag{1}$$

where $\mathcal{C}_i(\mu)$ denotes the Wilson coefficients at the renormalization scale μ, and $\mathcal{O}_i$ denotes a basis of field operators. The most relevant operators are

$$\begin{aligned}\mathcal{O}_{7(7')} &= \frac{m_b}{e}\left[\bar{s}\sigma^{\mu\nu}P_{R(L)}b\right] F_{\mu\nu}\,, \\ \mathcal{O}_{9(9')} &= \left[\bar{s}\gamma_\mu P_{L(R)}b\right]\left[\bar{\ell}\gamma^\mu\ell\right]\,, \\ \mathcal{O}_{10(10')} &= \left[\bar{s}\gamma_\mu P_{L(R)}b\right]\left[\bar{\ell}\gamma^\mu\gamma_5\ell\right]\,,\end{aligned} \tag{2}$$

where a primed index indicates a flip of the quarks' chiralities with respect to the unprimed, SM-like operator. Further four-quark operators $\mathcal{O}_i \sim [\bar{s}\Gamma_i b]\,[\bar{q}\Gamma_i' q]$, $i = 1, \ldots, 6$ as well as the chromomagnetic operator $\mathcal{O}_8$ contribute to the transition amplitudes via hadronic matrix elements of two-point correlators with the quark electromagnetic current. These contributions are taken into account in the numerical evaluation of the $b \to s\ell^+\ell^-$ observables via process- and q^2-dependent shifts of the effective Wilson coefficients $\mathcal{C}_{9,\lambda}$ and $\mathcal{C}_{7,\lambda}$ that enter in the various transversity amplitudes. The expressions relevant to this work can be taken from Refs. [18, 19] (for $\Lambda_b \to \Lambda\ell^+\ell^-$ at high q^2) and Ref. [20] (for $B \to X_s\ell^+\ell^-$ at low q^2). For definiteness, we fix $\mu = 4.2\,\text{GeV}$ in our fits.

* smeinel@email.arizona.edu
† dvandyk@physik.uzh.ch

A. Fit Models

For the purpose of our analysis we define three fit scenarios, labeled "SM(ν-only)", "$(9, 10)$", and "$(9, 9', 10, 10')$", respectively:

$$\begin{aligned}
\text{SM}(\nu\text{-only}) &: \begin{cases} \mathcal{C}_{7,9,10} & \text{SM values} \\ \mathcal{C}_{7',9',10'} & \text{SM values} \\ \vec{\nu} & \text{free floating} \end{cases}, \\
(9,10) &: \begin{cases} \mathcal{C}_{9} & \in [-4,+9] \\ \mathcal{C}_{10} & \in [-6,-2] \\ \mathcal{C}_{7,7',9',10'} & \text{SM values} \\ \vec{\nu} & \text{free floating} \end{cases}, \\
(9,9',10,10') &: \begin{cases} \mathcal{C}_{9,9',10,10'} & \in [-8,+8] \\ \mathcal{C}_{7,7'} & \text{SM values} \\ \vec{\nu} & \text{free floating} \end{cases},
\end{aligned} \tag{3}$$

where the parameters of interest are $\vec{\vartheta} = (\mathcal{C}_9, \mathcal{C}_{10})$ or $\vec{\vartheta} = (\mathcal{C}_9, \mathcal{C}_{9'}, \mathcal{C}_{10}, \mathcal{C}_{10'})$, and where the nuisance parameters $\vec{\nu}$ account for theoretical uncertainties in the computation of the observables[1]. We obtain the posterior density for a given model M, $P(\vec{x}\,|\,M, \text{data})$, using Bayes' theorem

$$P(\vec{x}\,|\,M, \text{data}) = \frac{P(\text{data}\,|\,\vec{x}, M) P_0(\vec{x}\,|\,M)}{P(\text{data}\,|\,M)}\,. \tag{4}$$

In the above, $\vec{x} \equiv (\vec{\vartheta}, \vec{\nu})$, $P_0(\vec{x}, M)$ is the prior density, and $P(\text{data}\,|\,\vec{x}, M)$ denotes the product of the experimental likelihoods. The prior density factorizes,

$$P_0(\vec{x}\,|\,M) \equiv P_0(\vec{\vartheta}\,|\,M) P_0(\vec{\nu}\,|\,M)\,, \tag{5}$$

into the prior for the parameters of interest, which is multivariate uniform (see eq. (3)), and the informative (i.e., non-uniform) priors for the nuisance parameters. The normalization on the right-hand side of eq. (4),

$$P(\text{data}\,|\,M) \equiv \int_{V(M)} \mathrm{d}\vec{x}\; P(\text{data}\,|\,\vec{x}, M) P_0(\vec{x}\,|\,M)\,, \tag{6}$$

is the total evidence of the data given the model M. We will refer to it as the *local evidence* whenever we restrict the integration hypervolume $V(M)$ to a subset of the support of $P_0(\vec{x}, M)$. The parameter point $\vec{x}^{\,*} \equiv (\vec{\vartheta}^{\,*}, \vec{\nu}^{\,*})$ maximizes the posterior,

$$\vec{x}^{\,*} = \arg\max_x P(\vec{x}\,|\,M, \text{data})\,, \tag{7}$$

and is referred to as the best-fit point. For the purpose of calculating the goodness of fit, we then compute

$$\chi^2 \equiv -2 \ln P(\text{data}\,|\,\vec{x}^{\,*}, M)\,. \tag{8}$$

[1] Note that our fit models are lepton-flavor-universal, and therefore cannot account for the present measurement of R_K [21].

Since all measurements enter the likelihood as univariate Gaussians, we define their individual *pull* values as

$$\text{pull}_i \equiv \frac{O - O(\vec{x}^{\,*})}{\sigma}\,, \tag{9}$$

in which $O \pm \sigma$ corresponds to the experimental results, and $O(\vec{x}^{\,*})$ denotes the theory prediction at the best-fit point.

In order to compare pairs of fit models, we employ the notion of posterior odds. The odds of model M_1 over model M_2 are defined as

$$\frac{P(M_1\,|\,\text{data})}{P(M_2\,|\,\text{data})} = \frac{P(\text{data}\,|\,M_1)}{P(\text{data}\,|\,M_2)} \frac{P_0(M_1)}{P_0(M_2)}\,. \tag{10}$$

In the above, $P_0(M)$ denotes a model prior. The latter can be obtained from, e.g., independent fits. In the absence of such results and following standard practice, we use identical priors for all our models: $P_0(M) \equiv 1 \,\forall\, M$.

Our statistical approach closely follows the one used in Refs. [6, 22]. The calculation of all observables (listed in the following subsection), and the statistical procedures are carried out through use of the EOS software [23], which implements a Monte Carlo algorithm as described in Ref. [24].

B. Inputs

Our fits take into account the following observables:

1. The main task is the inclusion of the branching ratio of $\Lambda_b \to \Lambda(\to p\,\pi^-)\mu^+\mu^-$ decays, as well as three further observables that arise from the angular distribution [19]: F_0, the rate of longitudinally-polarized lepton pairs, as well as the leptonic and the hadronic forward-backward asymmetries A_{FB}^{ℓ} and A_{FB}^{Λ}. The theory of QCD factorization at low q^2 [25] is not yet fully developed for the baryonic decay (see Ref. [26] for a recent discussion), and we therefore restrict our analysis to the high-q^2 region, where the usual low-recoil OPE [18, 27] is applicable. This restricts our use to observables that are integrated of the entire low recoil region, $15\,\text{GeV}^2 \leq q^2 \leq 20\,\text{GeV}^2 \simeq q^2_{\text{max}}$. We denote the binning in this range as $\langle\,\cdot\,\rangle_{15,20}$.

   The LHCb collaboration has published an analysis of both the branching ratio and the three aforementioned angular observables [15], which are all included in our likelihood. The CDF collaboration had previously reported [28] the first observation of this decay, and performed a measurement of its branching ratio. However, the CDF analysis is based on only a small number of 24 ± 5 signal candidates in the entire phase space; the uncertainty of the branching ratio in the low recoil region is accordingly large. The CDF result is compatible with the LHCb result, but with approximately

three times larger uncertainty. We therefore do not include the CDF measurement in our fits.

2. We denote the time-integrated branching ratio of the decay $B_s \to \mu^+\mu^-$ as $\int \mathrm{d}\tau\, \mathcal{B}(\tau)$ [29]. Our likelihood includes the recent results from a combined analysis of the CMS and LHCb collaborations [30]. All of our fit models, as specified in eq. (3), imply $A^{\mu\mu}_{\Delta\Gamma_s} = 1$ [29].

3. From the inclusive decay $B \to X_s\ell^+\ell^-$ we use the branching ratio, integrated over the range of dilepton mass square $1\,\mathrm{GeV}^2 \le q^2 \le 6\,\mathrm{GeV}^2$; denoted as $\langle\mathcal{B}\rangle_{1,6}$. The likelihood includes the measurements by the BaBar [31] and the Belle [32] [2] collaborations.

A summary of nuisance parameters, their association with specific observables, and their respective priors that enter our analyses is shown in table I.

The ten $\Lambda_b \to \Lambda$ form factors in the helicity basis are parametrized using simplified z expansions [33] of the form

$$f(q^2) = \frac{1}{1 - q^2/m^2_{\mathrm{pole},f}} \sum_{k=0}^{k_{\max}} a_{f,k}\,[z(q^2)]^k. \qquad (11)$$

The prior distribution of the parameters $\{a_{f,k}\}$ is a multivariate Gaussian given by the lattice QCD calculation of Ref. [16] (the definition of z and the values of the pole masses, $m_{\mathrm{pole},f}$, are also given in Ref. [16]). Note that Ref. [16] provides two sets of form factor parameters: the "nominal parameters" with $k_{\max} = 1$, which are used to evaluate central values and statistical uncertainties, and the "higher-order parameters" with $k_{\max} = 2$, which are used in combination with the nominal parameters to evaluate systematic uncertainties according to Eqs. (50)-(56) of Ref. [16]. Since a Bayesian fit requires a single fit model, we follow a simplified approach in this work. We use $k_{\max} = 2$ throughout, but set the central values of $a_{f,0}$ and $a_{f,1}$ equal to the nominal values and set the central values of $a_{f,2}$ to zero. We then compute the *total* (statistical plus systematic) covariance matrix of the parameters $\{a_{f,0}, a_{f,1}, a_{f,2}\}$ according to Eq. (56) of Ref. [16], and use this total covariance matrix in our prior distribution. In the high-q^2 region considered here, this simplified procedure accurately reproduces the total covariances of all form factors and observables as computed using the original method [16]. [3]

[2] In absence of a measurement for the $\mu^+\mu^-$ final state, we use the Belle result for a mixture of $\mu^+\mu^-$ and e^+e^- final states, assuming lepton universality.

[3] This is not the case in the low-q^2 region (which is not used here). At low q^2, the statistical and systematic uncertainties in the form factors are larger due to the absence of lattice data points in that region. Consequently, deviations from the quadratic approximation in Gaussian error propagation are larger, and the resulting estimates depend on the order of the steps taken.

Quantity	Prior	Unit	Reference
CKM Wolfenstein parameters			
A	0.806 ± 0.020	—	[34]
λ	0.2253 ± 0.0006	—	[34]
$\bar\rho$	0.132 ± 0.049	—	[34]
A	0.369 ± 0.050	—	[34]
Quark masses			
$\overline{m}_c(m_c)$	1.275 ± 0.025	GeV	[35]
$\overline{m}_b(m_b)$	4.18 ± 0.03	GeV	[35]
HQE parameters			
$\mu_\pi^2(1\,\mathrm{GeV})$	0.45 ± 0.10	GeV^2	[36]
$\mu_G^2(1\,\mathrm{GeV})$	$0.35^{+0.03}_{-0.02}$	GeV^2	[36]
B_s decay constant			
f_{B_s}	227.7 ± 4.5	MeV	[37–40]
$\Lambda \to p\,\pi^-$ decay parameter			
α	0.642 ± 0.013	—	[35]

TABLE I. Prior distributions of selected nuisance parameters: CKM parameters, quark masses, hadronic matrix elements entering the inclusive and the exclusive leptonic decays, and $\Lambda \to p\,\pi^-$ parity-violating decay parameter. For the CKM parameters, we use the results of a Bayesian analysis of only tree-level decays, which was performed by the UTfit Collaboration in 2013 [34]. All distributions are Gaussian, with the exception of $\mu_G^2(1\,\mathrm{GeV})$. The latter follows a LogGamma distribution whose additional parameter allows to faithfully reproduce the asymmetric uncertainty interval as given in [36]. The prior distribution for the $\Lambda_b \to \Lambda$ form factors is a multivariate Gaussian with inputs directly taken from the lattice QCD calculation in Ref. [16]; see the text for details.

III. RESULTS

In the following subsections we will summarize our findings for each of the fit scenarios through

- the value of $\vec\vartheta^*$, the best-fit point for the parameters of interest (if applicable);
- a summary of $\vec\nu^*$, the nuisance parameters at the best-fit point, as well as a summary of the 1D-marginalizd densities of the posterior for all components of $\vec\nu$;
- a χ^2 value and its associated p-value: our a-priori threshold for an acceptable fit is $p \ge 0.03$;
- a description of a hypercube that includes the global mode of the posterior, and its associated local evidence;
- and a summary of the 1D-marginalized posteriors of the parameters of interest for the local solution with the largest local evidence.

Constraint	Pull value [σ] SM(ν-only)	$(9, 10)$	$(9, 9', 10, 10')$
$\Lambda_b \to \Lambda\mu^+\mu^-$			
$\langle\mathcal{B}\rangle_{15,20}$	+0.86	−0.17	−0.08
$\langle F_0\rangle_{15,20}$	+1.41	+1.41	+1.41
$\langle A_{\rm FB}^{\ell}\rangle_{15,20}$	+3.13	+2.60	+0.72
$\langle A_{\rm FB}^{\Lambda}\rangle_{15,20}$	−0.26	−0.24	−1.08
$\bar{B}_s \to \mu^+\mu^-$			
$\int \mathrm{d}\tau\, \mathcal{B}(\tau)$	−0.72	+0.75	+0.37
$\bar{B} \to X_s\ell^+\ell^-$			
$\langle\mathcal{B}\rangle_{1,6}$ (BaBar)	+0.47	−0.26	−0.10
$\langle\mathcal{B}\rangle_{1,6}$ (Belle)	+0.17	−0.35	−0.24
	χ^2 at best-fit point		
	13.40	9.60	3.87

TABLE II. Pull values for the individual experimental constraints within each of the fit scenarios at the respective best-fit point. The last line gives the total χ^2 value at the respective best-fit point.

A short summary of the goodness-of-fit quantities for each of the scenarios is shown in table II .

A. Scenario SM(ν-only)

This scenario does not feature any parameters of interest, and thus only probes the goodness-of-fit between the theory predictions in the SM and the data. We find that both the best-fit point $\vec{\nu}^*$ and the 1D-marginalized posterior densities correspond excellently to the prior density for each of the 35 nuisance parameters. Overall, we find $\chi^2 = 13.40$ for 7 degrees of freedom (d.o.f.). This translates to a p-value of 0.06, assuming a Gaussian likelihood. Since this value is larger than our a-priori threshold for the p-value, we accept this fit. We obtain the global evidence as $P(\text{data}\,|\,\text{SM}(\nu\text{-only})) = (1.1469 \pm 0.0003)\cdot 10^{18}$, where the error is only statistical in nature[4]. The individual pull values for this scenario are listed in the left column of table II. We draw attention to the observable $\langle A_{\rm FB}^{\ell}\rangle_{15,20}$, whose pull is the only pull to exceed 3σ; all other pulls are smaller than 2σ.

[4] Large numbers for the evidence are not worrisome. They are driven by the integration of the likelihood as a function of the model parameters over the model parameters. As such, they are meaningful for comparison of fits as long as the fits share the same likelihood. Providing the evidence as part of our analysis allows other researchers to make their own conclusions, and to produce their own Bayes factors for model comparisons.

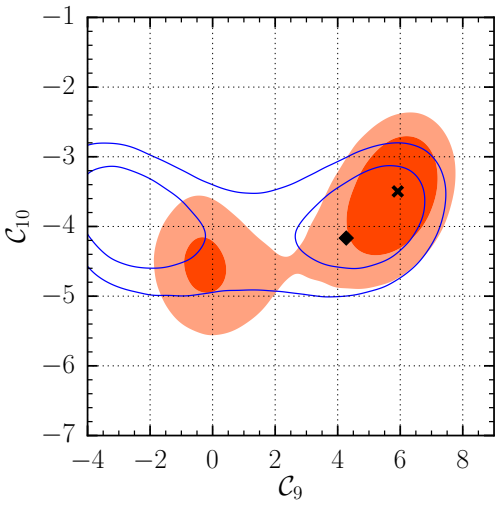

FIG. 1. The 2D-marginalised posterior in the $\mathcal{C}_9$-$\mathcal{C}_{10}$ plane. To demonstrate the impact of including the baryonic decay in the analysis, we show the results from a fit to the $\bar{B} \to X_s\ell^+\ell^-$ and $\bar{B}_s \to \mu^+\mu^-$ branching ratios only (blue lines) and from the full fit including also the $\Lambda_b \to \Lambda(\to p\,\pi^-)\mu^+\mu^-$ observables (orange-red areas). The SM point is marked with a diamond shape, while the best-fit point from the full fit is marked with a black cross. The contours correspond to 68% (inner contours) and 95% (outer contours) of probability for the respective 2D-marginalised posteriors.

B. Scenario (9,10)

In this scenario we fit 2 parameters of interest in addition to the parameters of SM(ν-only). The ϑ components of the best-fit point read

$$\vec{\vartheta}^*: (\mathcal{C}_9, \mathcal{C}_{10}) = (5.92, -3.50)\,. \tag{12}$$

The 2D marginalization onto these two parameter is shown in figure 1. As before for the model SM(ν-only), we find that also in this fit model the nuisance parameters $\vec{\nu}^*$ and their 1D-marginalized posterior densities correspond excellently to the priors densities. We further obtain $\chi^2 = 9.60$, which is a reduction compared to SM(ν-only) by 3.80. Given the now 5 d.o.f., we find a p-value of 0.09; the fit is therefore acceptable. The evidence is $P(\text{data}\,|\,(9,10)) = (2.253 \pm 0.008)\cdot 10^{17}$. The most prominent local mode lies within the rectangle

$$+3 \le \mathcal{C}_9 \le +9 \quad -6 \le \mathcal{C}_{10} \le -2\,, \tag{13}$$

which contributes $(1.738 \pm 0.008)\cdot 10^{17}$ or roughly 77% to the evidence. The 1D marginal posteriors for both $\mathcal{C}_9$ and $\mathcal{C}_{10}$ are non-Gaussian, and we find for their respective modes and 1σ intervals:

$$\begin{aligned} \mathcal{C}_9 &= +5.9^{+0.7}_{-0.9}\,, \quad \Delta_9 = +1.6^{+0.7}_{-0.9}\,, \\ \mathcal{C}_{10} &= -3.5^{+0.5}_{-0.8}\,, \quad \Delta_{10} = +0.7^{+0.5}_{-0.8}\,. \end{aligned} \tag{14}$$

In the above, we also state the ranges for $\Delta_i \equiv \mathcal{C}_i - \mathcal{C}_i^{\rm SM}$ for $i = 9, 10$. A comparison of our results with other

findings in the literature is difficult, due to the different methodologies. Naively, one finds that the maximum distance between our results and the ones from Refs. [6, 9, 13] are

$$-3.1\sigma \text{ for } \Delta_9 \qquad \text{and} \qquad -1.1\sigma \text{ for } \Delta_{10}, \tag{15}$$

where we have expressed the distance in terms of the width of our results for 68% probability intervals.

In conclusion, we find that, while the (9,10) scenario can locally explain the data better by a $\Delta\chi^2 = 3.80$, on average the SM(ν-only) scenario is more efficient in explaining the data with posterior odds

$$\frac{P((9,10)\,|\,\text{data})}{P(\text{SM}(\nu\text{-only})\,|\,\text{data})} = 1:6.6\,. \tag{16}$$

Following Jeffreys' scale [41] these odds are *substantially* in favor of SM(ν-only).

C. Scenario (9,10,9',10')

For this scenario we fit four parameters of interest in addition to the nuisance parameters, yielding 39 fit parameters. The ϑ components of the best-fit point are

$$\vec{\vartheta}^*: (\mathcal{C}_9, \mathcal{C}_{9'}, \mathcal{C}_{10}, \mathcal{C}_{10'}) = (6.20, 0.50, -1.13, +2.54)\,. \tag{17}$$

We show all 2D marginalizations of the posterior in figure 2. As in Ref. [24], we find four local solutions. However, opposed to the results of Ref. [24], the local solutions in our posterior are not well separated in the 2D marginalizations. We interpret this as an effect of a "shallow" posterior, which is due to the still considerable uncertainties on the experimental results for the $\Lambda_b \to \Lambda$ observables, and also the small number of observations: a full angular analysis of the decay $\Lambda_b \to \Lambda(\to p\,\pi^-)\mu^+\mu^-$ is therefore desirable. As a further consequence, the posterior of the nuisance parameters is very close to our prior. At the best-fit point we find $\chi^2 = 3.87$, which is a reduction compared to the $(9,10)$ scenario by 5.73, and compared to SM(ν-only) by 9.53. Given the only 3 degrees of freedom in this exploratory scenario, we obtain a p-value of 0.28, which is a good fit. We obtain for the evidence $P(\text{data}\,|\,(9,9',10,10')) = (2.188 \pm 0.003)\cdot 10^{16}$, with the uncertainty only due to statistics.

We proceed to investigate one of the four solutions that is contained within the hyperrectangle

$$\begin{aligned} +3 \le \mathcal{C}_9 \le +8\,, \quad & -4 \le \mathcal{C}_{9'} \le +4\,, \\ -4 \le \mathcal{C}_{10} \le +1\,, \quad & 0 \le \mathcal{C}_{10'} \le +5\,. \end{aligned} \tag{18}$$

Its local evidence is found to be $(1.152 \pm 0.001)\cdot 10^{16}$, which corresponds to $\sim 53\%$ of the total evidence. We obtain the 1D marginalizations within the above boundaries, which are non-Gaussian. The modes and 1σ intervals read

$$\begin{aligned} \mathcal{C}_9 &= +6.0^{+0.8}_{-0.8}\,, \quad & \Delta_9 &= +1.7^{+0.8}_{-0.8}\,, \\ \mathcal{C}_{9'} &= +0.5^{+1.3}_{-1.8}\,, & & \\ \mathcal{C}_{10} &= -1.3^{+1.3}_{-1.1}\,, & \Delta_{10} &= +2.9^{+1.3}_{-1.1}\,, \\ \mathcal{C}_{10'} &= +2.3^{+0.8}_{-1.3}\,, & & \end{aligned} \tag{19}$$

where, as before, $\Delta_i \equiv \mathcal{C}_i - \mathcal{C}_i^{\text{SM}}$.

Our findings can be summarized as follows: The posterior odds relative to the previous two fit scenarios are

$$\frac{P((9,9',10,10')\,|\,\text{data})}{P(\text{SM}(\nu\text{-only})\,|\,\text{data})} = 1:100\,, \tag{20}$$

as well as

$$\frac{P((9,9',10,10')\,|\,\text{data})}{P((9,10)\,|\,\text{data})} = 1:15\,. \tag{21}$$

Thus, again, SM(ν-only) is more efficient in its description of the data than a new-physics interpretation involving $\mathcal{C}_9$ through $\mathcal{C}_{10'}$.

IV. DISCUSSION

The newly available lattice QCD results for the $\Lambda_b \to \Lambda$ form factors [16] have considerably decreased the theoretical uncertainties in the $\Lambda_b \to \Lambda(\to p\,\pi^-)\mu^+\mu^-$ observables at low hadronic recoil, and the strengths of the constraints on the $|\Delta B| = |\Delta S| = 1$ Wilson coefficients are currently limited by the experimental uncertainties. Nevertheless, already with the current experimental data [15], we find that this decay has now reached a similar level of constraining power as the decay $\bar{B} \to \bar{K}^*\mu^+\mu^-$ exhibited after the first LHCb measurement [42].

Within our nominal fit in the $(9,10)$ scenario, we find

$$\begin{aligned} \mathcal{C}_9 &= +5.9^{+0.7}_{-0.9}\,, \quad & \Delta_9 &= +1.6^{+0.7}_{-0.9}\,, \\ \mathcal{C}_{10} &= -3.5^{+0.5}_{-0.8}\,, & \Delta_{10} &= +0.7^{+0.5}_{-0.8}\,. \end{aligned} \tag{22}$$

Our fits in both the $(9,10)$ and $(9,9',10,10')$ scenarios were surprisingly well behaved, given the small number of observables included. We look forward to including the $\Lambda_b \to \Lambda(\to p\,\pi^-)\mu^+\mu^-$ data in a larger analysis together with all mesonic decays.

Even though our fits of the Wilson coefficients yield noticeable reductions in χ^2 compared to the SM, neither the scenario $(9,10)$, nor the scenario $(9,9',10,10')$, is as *efficient* as the Standard Model in describing the combined present data on inclusive $B \to X_s\ell^+\ell^-$ decays, the leptonic decay $B_s \to \mu^+\mu^-$, and the branching ratio and angular observables of $\Lambda_b \to \Lambda(\to p\,\pi^-)\mu^+\mu^-$. As a consequence, we find no evidence for effects of physics beyond the Standard Model.

When comparing our results for the Wilson coefficient $\mathcal{C}_9$ with analyses excluding the baryonic decay but including the decays $\bar{B} \to \bar{K}^{(*)}\mu^+\mu^-$, we find poor agreement

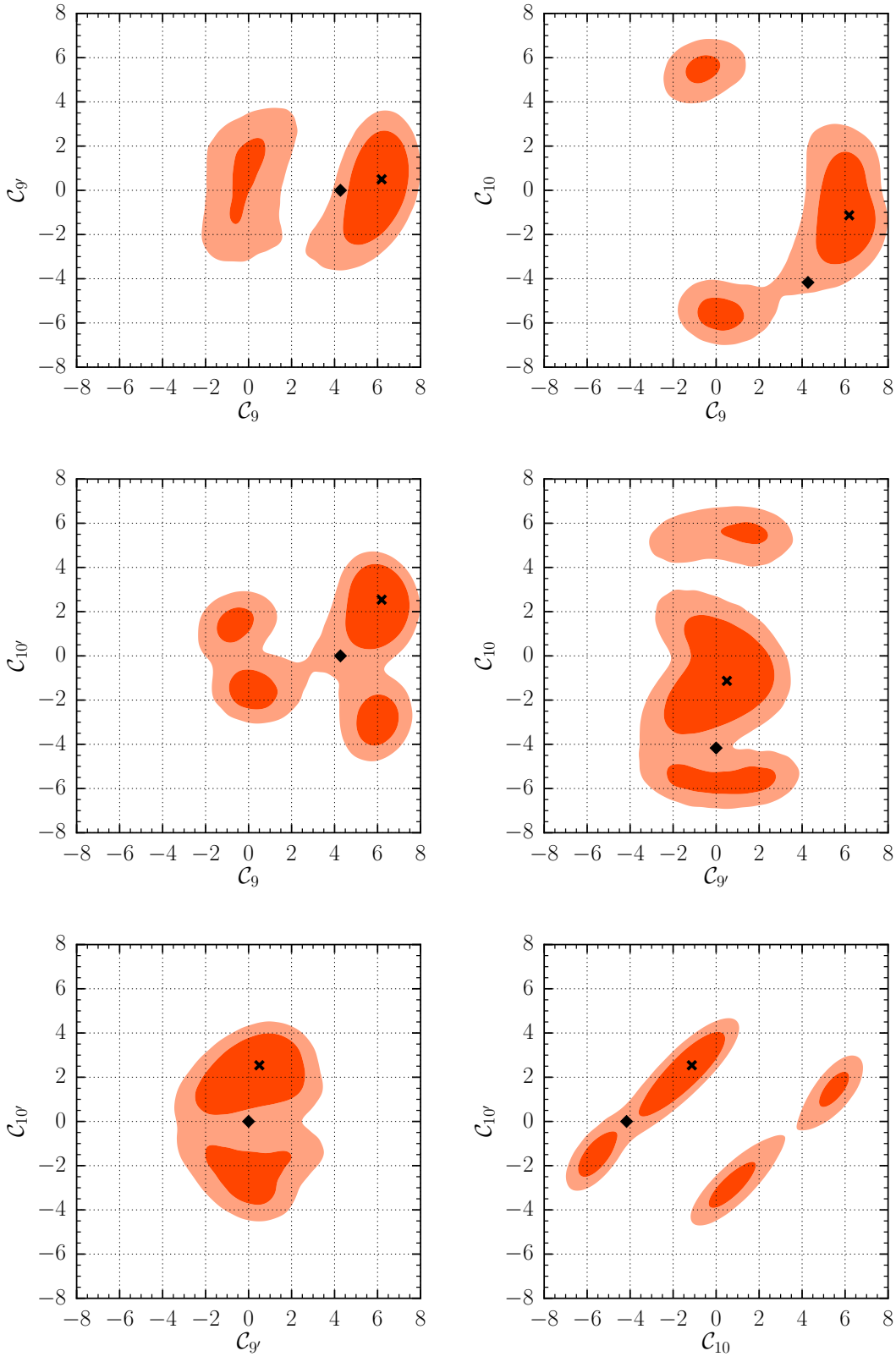

FIG. 2. The 2D-marginalised posteriors for all pairs of Wilson coefficients in the $(9, 10, 9', 10')$ scenario. The SM point is marked with a diamond shape, while the best-fit point from the full fit is marked with a black cross. The contours correspond to 68% (inner contours) and 95% (outer contours) of probability for the respective 2D-marginalised posteriors.

with the findings in the literature. The maximal distance emerges for the most recent result of Ref. [13], and reads -3.1σ in terms of the standard deviation of our result.

In our opinion, the observed discrepancy can be caused by two different mechanisms:

1. The discrepancy might arise from our incomplete understanding of the hadronic matrix elements of the two-point correlators of $\mathcal{O}_{1,\dots,6;8}$ with the quark electromagnetic current, which effectively shift the Wilson coefficients $\mathcal{C}_7$ and $\mathcal{C}_9$. The main difficulty arises from the operators $\mathcal{O}_1$ and $\mathcal{O}_2$, whose contributions are enhanced by charmonium resonances (see e.g. Ref. [43], where these contributions are discussed within a hadronic dispersion relation). A drastically different shift to $\mathcal{C}_9$ in the baryonic decay compared to the mesonic transitions, e.g. through different phases, would yield the different results that we currently face. This would constitute a breakdown of the universal structure of the transversity amplitudes at low recoil [19, 44] that is predicted by the OPE. We explicitly show in appendix C that such effects can only partially explain the presently observed shift to $\mathcal{C}_9$.

2. Given the large experimental uncertainties for the $\Lambda_b \to \Lambda(\to p\,\pi^-)\mu^+\mu^-$ observables, statistical fluctuations could conspire to mimic a large positive shift to $\mathcal{C}_9$. The best candidate for such an influence in the fit is the measurement of the branching ratio $\langle\mathcal{B}\rangle_{15,20}$. We note that the experimental uncertainty of $\langle\mathcal{B}\rangle_{15,20}$ [15] is currently dominated by the uncertainty of the branching ratio of the normalization mode $\Lambda_b \to J/\psi\,\Lambda$ [35].

One must also consider that the results of Ref. [13] are driven, amongst other effects, by the low value of R_K [21], which cannot be explained by hadronic effects, and the consistent picture of the mesonic decays $\bar{B} \to \bar{K}^{(*)}\mu^+\mu^-$ both below and above the narrow charmonium resonances.

Ultimately, to settle the questions regarding $\mathcal{C}_9$, we need both a reduction in the experimental uncertainties for $\Lambda_b \to \Lambda(\to p\,\pi^-)\mu^+\mu^-$ (and an analysis of the full angular distribution, e.g. using a principal moment analysis as proposed in [45]) as well as breakthroughs in our understanding of the nonlocal hadronic matrix elements of the operators $\mathcal{O}_{1,\dots,6;8}$.

ACKNOWLEDGMENTS

The work of S.M. is supported by National Science Foundation Grant Number PHY-1520996, and by the RHIC Physics Fellow Program of the RIKEN BNL Research Center. The work of D.v.D. is supported by the Swiss National Science Foundation, grant PP00P2-144674. We thank Christoph Bobeth, Joaquim Matias, Luca Silvestrini and Roman Zwicky for useful comments on our preliminary results that were presented during the "4th Workshop on Implications of LHCb measurements and future prospects".

Appendix A: Parametrization of subleading terms in the low recoil OPE

The decay $\Lambda_b \to \Lambda\ell^+\ell^-$ can be described through eight transversity amplitudes: $A^L_{\perp_0}$, $A^L_{\parallel_0}$, $A^L_{\perp_1}$, $A^L_{\parallel_1}$, and their counterparts with $L \leftrightarrow R$. At low recoil, the OPE predicts a universal structure, see [19]. Following Ref. [18], this structure is broken only by hadronic matrix elements r_i (where $i \in \{\perp_0, \parallel_0, \perp_1, \parallel_1\}$) at the level of dimension-five operators in the OPE. We therefore write the transversity amplitudes as

$$
\begin{aligned}
A^{L(R)}_{\perp_0} &= +\sqrt{2}N\sqrt{s_-}\frac{m_{\Lambda_b}+m_\Lambda}{\sqrt{q^2}}\left[C^{L(R)}_{9,10,+}\,f_0^V + \frac{2m_b(C_7+C_{7'})}{m_{\Lambda_b}+m_\Lambda}f_0^T \;+\left(\frac{4}{3}C_1+C_2\right)r_{\perp_0}\right],\\
A^{L(R)}_{\parallel_0} &= -\sqrt{2}N\sqrt{s_+}\frac{m_{\Lambda_b}-m_\Lambda}{\sqrt{q^2}}\left[C^{L(R)}_{9,10,-}\,f_0^A + \frac{2m_b(C_7-C_{7'})}{m_{\Lambda_b}-m_\Lambda}f_0^{T5} + \left(\frac{4}{3}C_1+C_2\right)r_{\parallel_0}\right],\\
A^{L(R)}_{\perp_1} &= -2N\sqrt{s_-}\left[C^{L(R)}_{9,10,+}\,f_\perp^V + \frac{2m_b(m_{\Lambda_b}+m_\Lambda)(C_7+C_{7'})}{q^2}f_\perp^T \;+\left(\frac{4}{3}C_1+C_2\right)r_{\perp_1}\right],\\
A^{L(R)}_{\parallel_1} &= +2N\sqrt{s_+}\left[C^{L(R)}_{9,10,+}\,f_\perp^A + \frac{2m_b(m_{\Lambda_b}-m_\Lambda)(C_7-C_{7'})}{q^2}f_\perp^{T5} \;+\left(\frac{4}{3}C_1+C_2\right)r_{\parallel_1}\right],
\end{aligned}
\tag{A1}
$$

where the kinematics quantities $s_\pm$, the effective Wilson coefficients $C^{L(R)}_{9,10,\pm}$, the normalization N, and the formfactors f^J_λ are defined as in Ref. [19].

In general, the matrix elements r_i are complex-valued, q^2-dependent functions. These matrix elements arise only with a suppression of order $\Lambda^2_{\rm had}/Q^2$, where $Q^2 \sim \{m_b^2, q^2\}$. (We note that a similar parametrization is used

Observable	$(9,10)$
$\hat{K}_{1ss}$	$+0.352^{+0.003}_{-0.003}$
$\hat{K}_{1cc}$	$+0.296^{+0.006}_{-0.006}$
$\hat{K}_{1c}$	$-0.233^{+0.008}_{-0.008}$
$\hat{K}_{2ss}$	$-0.195^{+0.005}_{-0.005}$
$\hat{K}_{2cc}$	$-0.153^{+0.006}_{-0.006}$
$\hat{K}_{2c}$	$+0.186^{+0.004}_{-0.004}$
$\hat{K}_{4sc}$	$-0.022^{+0.005}_{-0.005}$
$\hat{K}_{4s}$	$-0.102^{+0.007}_{-0.009}$

TABLE III. Summary of the 1D marginalised posterior-predictive distributions for the normalized angular observables $\hat{K}_n = \langle K_n\rangle_{15,20}/\langle\Gamma\rangle_{15,20}$. We present the distributions obtained from the posteriors of the $(9,10)$ scenario. The statistical uncertainty from the Monte Carlo integration is estimated to be 10^{-3}.

in Ref. [46]. However, there the OPE is used in terms of HQET operators [27]. As a consequence, the leading corrections to the OPE arise from dimension-four operators, which enter suppressed by one power of the strong coupling α_s. As such, their effect is virtually the same as here.)

Since in our fits we only use a single q^2 bin that covers the entire phase space above $q^2 = 15\,\text{GeV}^2$, we can parametrize the unknown hadronic matrix elements as q^2-constant quantities. Within the fits, we take the r_i to be real-valued[5], with *uncorrelated* Gaussian priors centered around zero and with a standard deviation of 0.03: $r_i \sim \mathcal{N}(0, 0.03)$. We emphasize that this is a conservative estimate for the size of these hadronic matrix elements, since $\Lambda^2_{\text{had}}/Q^2 \lesssim 0.9\%$.

Appendix B: Posterior-predictive distributions for the $\Lambda_b \to \Lambda(\to p\,\pi^-)\mu^+\mu^-$ angular observables

In this section, we compute posterior-predictive distributions for the normalized angular observables

$$\hat{K}_n \equiv \frac{\langle K_n\rangle_{15,20}}{\langle\Gamma\rangle_{15,20}}\,, \tag{B1}$$

from the $(9,10)$ fit scenario. Summaries in form of the mode and the 68% probability interval for the observables with $n \in \{1ss, 1cc, 1c, 2ss, 2cc, 2c, 4sc, 4s\}$ are shown in table III. We abstain from providing predictions for the observables with $n \in \{3sc, 3s\}$, since for real-valued Wilson coefficients these observables are only sensitive to small interference effects introduced by the imaginary parts of the hadronic matrix elements of $\mathcal{O}_{1,\dots,6;8}$, and by the contributions proportional to V_{ub}.

[5] Only the observables K_{3sc} and K_{3s}, or combinations thereof, are sensitive to the phases of the matrix elements r_i. As these observables are presently unconstrained, our use of real-valued quantities therefore suffices. A similar observation has been made in [6] for power corrections at large q^2 in $B \to K^{(*)}\mu^+\mu^-$ decays.

Appendix C: Fits of $\Lambda_b \to \Lambda(\to p\,\pi^-)\mu^+\mu^-$ data only

In order to further investigate a possible hadronic origin for the tensions between theory and experiment, we carry out fits to only the $\Lambda_b \to \Lambda(\to p\,\pi^-)\mu^+\mu^-$ observables listed in table II. Beside the scenario SM(ν-only), we also employ a new scenario (9):

$$(9): \begin{cases} \mathcal{C}_9 & \in [-4,+9] \\ \mathcal{C}_{7,7',9',10,10'} & \text{SM values} \\ \vec{\nu} & \text{free floating} \end{cases}. \tag{C1}$$

Using the very same priors as described in section II, we find poor fits: When only fitting the nuisance parameters, the p-value is $1.3\cdot10^{-2}$, while the fit with freely floating $\mathcal{C}_9$ only slightly improves the p-value to $1.5\cdot10^{-2}$. The reason for this behavior is that the current experimental results for the observables $\langle\mathcal{B}\rangle_{15,20}$ and $\langle A^\ell_{\text{FB}}\rangle_{15,20}$ pull $\mathcal{C}_9$ in opposite directions (the branching ratio $\langle\mathcal{B}\rangle_{15,20}$, which more strongly depends on $\mathcal{C}_9$, favors a positive shift).

We thus investigate the possibility that hadronic effects break the universal nature of the OPE for the transversity amplitudes in $\Lambda_b \to \Lambda\mu^+\mu^-$ transitions. This corresponds to a breakdown of the semi-local quark-hadron duality. We can simulate such effects by dramatically increasing the allowed ranges of the power corrections r_i as defined in appendix A. We let $r_i \sim \mathcal{N}(0,3)$, on a support $-5 \le r_i \le +5$. Using these priors, we repeat our fits to only the $\Lambda_b \to \Lambda(\to p\,\pi^-)\mu^+\mu^-$ observables.

For the SM(ν-only) scenario with the wide priors for r_i we obtain $\chi^2 = 4.27$, and a p-value of 0.37. All 1D-posteriors of the form factor parameters, CKM parameters and quark masses are in agreement with their priors. The posteriors for the power correction parameters can be summarized as follows:

$$\begin{aligned} r_{\perp,0} &= +2.1^{+2.4}_{-2.2}\,, \\ r_{\parallel,0} &= +3.6^{+1.4}_{-1.8}\,, \\ r_{\perp,1} &= -3.2^{+2.1}_{-1.8}\,, \\ r_{\parallel,1} &= -1.5^{+2.2}_{-2.5}\,. \end{aligned} \tag{C2}$$

The total evidence is $P(\text{only } \Lambda_b \to \Lambda\mu^+\mu^- \,|\, \text{SM}(\nu\text{-only})) = 1.8\cdot10^5$.

For the scenario (9) with the wide priors for r_i we obtain $\chi^2 = 4.59$, and a p-value of 0.20. This is surprising at first glance, since it means that adding one parameter has lead to an *increase* in χ^2. However, $-\log P(\vec{x}^* \,|\, (9), \text{only } \Lambda_b \to \Lambda\mu^+\mu^-)$ has in fact *decreased* by 4.35 on the log scale. With respect to SM(ν-only), the r_i components of the best-fit point have moved closer to 0, thereby increasing the posterior. At the same time, a shift of $\Delta_9 = 0.7^{+1.5}_{-1.3}$ compensates for the smaller values

of the parameters r_i. The 1D posteriors of the power corrections read:

$$\begin{aligned} r_{\perp,0} &= +1.8^{+2.4}_{-2.5}\,, \\ r_{\parallel,0} &= +2.9^{+1.9}_{-1.9}\,, \\ r_{\perp,1} &= -3.4^{+2.4}_{-1.6}\,, \\ r_{\parallel,1} &= -2.5^{+2.3}_{-2.0}\,. \end{aligned} \tag{C3}$$

Compared to the shift $\Delta_9\Big|_{(9,10)} = 1.6^{+0.7}_{-0.9}$, we see a marked reduction in need to modify $\mathcal{C}_9$. We conclude that symmetry-breaking shifts to all four transversity amplitudes in $\Lambda_b \to \Lambda\mu^+\mu^-$ can only partially explain our results in the $(9, 10)$ scenario.

[1] R. Aaij *et al.* (LHCb), Phys. Rev. Lett. **111**, 191801 (2013), arXiv:1308.1707 [hep-ex].
[2] R. Aaij *et al.* (LHCb), (2015), arXiv:1512.04442 [hep-ex].
[3] S. Descotes-Genon, J. Matias, M. Ramon, and J. Virto, JHEP **01**, 048 (2013), arXiv:1207.2753 [hep-ph].
[4] S. Descotes-Genon, J. Matias, and J. Virto, Phys. Rev. **D88**, 074002 (2013), arXiv:1307.5683 [hep-ph].
[5] W. Altmannshofer and D. M. Straub, Eur. Phys. J. **C73**, 2646 (2013), arXiv:1308.1501 [hep-ph].
[6] F. Beaujean, C. Bobeth, and D. van Dyk, Eur. Phys. J. **C74**, 2897 (2014), [Erratum: Eur. Phys. J.C74,3179(2014)], arXiv:1310.2478 [hep-ph].
[7] R. R. Horgan, Z. Liu, S. Meinel, and M. Wingate, Phys. Rev. Lett. **112**, 212003 (2014), arXiv:1310.3887 [hep-ph].
[8] T. Hurth and F. Mahmoudi, JHEP **04**, 097 (2014), arXiv:1312.5267 [hep-ph].
[9] W. Altmannshofer and D. M. Straub, Eur. Phys. J. **C75**, 382 (2015), arXiv:1411.3161 [hep-ph].
[10] T. Hurth, F. Mahmoudi, and S. Neshatpour, JHEP **12**, 053 (2014), arXiv:1410.4545 [hep-ph].
[11] F. Beaujean, C. Bobeth, and S. Jahn, Eur. Phys. J. **C75**, 456 (2015), arXiv:1508.01526 [hep-ph].
[12] D. Du, A. X. El-Khadra, S. Gottlieb, A. S. Kronfeld, J. Laiho, E. Lunghi, R. S. Van de Water, and R. Zhou, Phys. Rev. **D93**, 034005 (2016), arXiv:1510.02349 [hep-ph].
[13] S. Descotes-Genon, L. Hofer, J. Matias, and J. Virto, (2015), arXiv:1510.04239 [hep-ph].
[14] T. Hurth, F. Mahmoudi, and S. Neshatpour, (2016), arXiv:1603.00865 [hep-ph].
[15] R. Aaij *et al.* (LHCb), JHEP **06**, 115 (2015), arXiv:1503.07138 [hep-ex].
[16] W. Detmold and S. Meinel, Phys. Rev. **D93**, 074501 (2016), arXiv:1602.01399 [hep-lat].
[17] C. Bobeth, G. Hiller, and D. van Dyk, Phys. Rev. **D87**, 034016 (2013), arXiv:1212.2321 [hep-ph].
[18] M. Beylich, G. Buchalla, and T. Feldmann, Eur. Phys. J. **C71**, 1635 (2011), arXiv:1101.5118 [hep-ph].
[19] P. Böer, T. Feldmann, and D. van Dyk, JHEP **01**, 155 (2015), arXiv:1410.2115 [hep-ph].
[20] T. Huber, E. Lunghi, M. Misiak, and D. Wyler, Nucl. Phys. **B740**, 105 (2006), arXiv:hep-ph/0512066 [hep-ph].
[21] R. Aaij *et al.* (LHCb), Phys. Rev. Lett. **113**, 151601 (2014), arXiv:1406.6482 [hep-ex].
[22] F. Beaujean, C. Bobeth, D. van Dyk, and C. Wacker, JHEP **08**, 030 (2012), arXiv:1205.1838 [hep-ph].
[23] D. van Dyk *et al.*, "EOS - A HEP Program for Flavour Observables," (2016).
[24] F. Beaujean, *A Bayesian analysis of rare B decays with advanced Monte Carlo methods*, Ph.D. thesis, Fakultät für Physik, Technische Universität München (2012).
[25] M. Beneke, T. Feldmann, and D. Seidel, Nucl. Phys. **B612**, 25 (2001), arXiv:hep-ph/0106067 [hep-ph].
[26] Y.-M. Wang and Y.-L. Shen, (2015), 10.1007/JHEP02(2016)179, arXiv:1511.09036 [hep-ph].
[27] B. Grinstein and D. Pirjol, Phys. Rev. **D70**, 114005 (2004), arXiv:hep-ph/0404250 [hep-ph].
[28] T. Aaltonen *et al.* (CDF), Phys. Rev. Lett. **107**, 201802 (2011), arXiv:1107.3753 [hep-ex].
[29] K. De Bruyn, R. Fleischer, R. Knegjens, P. Koppenburg, M. Merk, A. Pellegrino, and N. Tuning, Phys. Rev. Lett. **109**, 041801 (2012), arXiv:1204.1737 [hep-ph].
[30] V. Khachatryan *et al.* (LHCb, CMS), Nature **522**, 68 (2015), arXiv:1411.4413 [hep-ex].
[31] J. P. Lees *et al.* (BaBar), Phys. Rev. Lett. **112**, 211802 (2014), arXiv:1312.5364 [hep-ex].
[32] M. Iwasaki *et al.* (Belle), Phys. Rev. **D72**, 092005 (2005), arXiv:hep-ex/0503044 [hep-ex].
[33] C. Bourrely, I. Caprini, and L. Lellouch, Phys. Rev. **D79**, 013008 (2009), [Erratum: Phys. Rev.D82,099902(2010)], arXiv:0807.2722 [hep-ph].
[34] M. Bona *et al.* (UTfit Collaboration), JHEP **0610**, 081 (2006), we use the updated data from Winter 2013 (pre-Moriond 13), arXiv:hep-ph/0606167 [hep-ph].
[35] K. A. Olive *et al.* (Particle Data Group), Chin. Phys. **C38**, 090001 (2014).
[36] N. Uraltsev, Phys. Lett. **B545**, 337 (2002), arXiv:hep-ph/0111166 [hep-ph].
[37] J. Laiho, E. Lunghi, and R. S. Van de Water, Phys. Rev. **D81**, 034503 (2010), arXiv:0910.2928 [hep-ph].
[38] A. Bazavov *et al.* (Fermilab Lattice, MILC), Phys. Rev. **D85**, 114506 (2012), arXiv:1112.3051 [hep-lat].
[39] C. McNeile, C. T. H. Davies, E. Follana, K. Hornbostel, and G. P. Lepage, Phys. Rev. **D85**, 031503 (2012), arXiv:1110.4510 [hep-lat].
[40] H. Na, C. J. Monahan, C. T. H. Davies, R. Horgan, G. P. Lepage, and J. Shigemitsu, Phys. Rev. **D86**, 034506 (2012), arXiv:1202.4914 [hep-lat].
[41] H. Jeffreys, *The Theory of Probability*, 3rd ed. (Oxford University Press, 1998).
[42] R. Aaij *et al.* (LHCb), Phys. Rev. Lett. **108**, 181806 (2012), arXiv:1112.3515 [hep-ex].
[43] A. Khodjamirian, T. Mannel, A. A. Pivovarov, and Y. M. Wang, JHEP **09**, 089 (2010), arXiv:1006.4945 [hep-ph].
[44] C. Bobeth, G. Hiller, and D. van Dyk, JHEP **07**, 098 (2010), arXiv:1006.5013 [hep-ph].
[45] F. Beaujean, M. Chrzaszcz, N. Serra, and D. van Dyk, Phys. Rev. **D91**, 114012 (2015), arXiv:1503.04100 [hep-ex].
[46] C. Bobeth, G. Hiller, and D. van Dyk, JHEP **07**, 067 (2011), arXiv:1105.0376 [hep-ph].